
Article:
LaBelle, J., Yearby, K. orcid.org/0000-0002-7605-4393 and Pickett, J.S. (2022) South Pole Station ground-based and Cluster satellite measurements of leaked and escaping Auroral Kilometric Radiation. Journal of Geophysical Research: Space Physics, 127 (2). e2021JA029399. ISSN 2169-9380

https://doi.org/10.1029/2021ja029399

JGR Space Physics

RESEARCH ARTICLE
10.1029/2021JA029399

Special Section:
Cluster 20th anniversary: results from the first 3D mission

South Pole Station Ground-Based and Cluster Satellite Measurements of Leaked and Escaping Auroral Kilometric Radiation

James LaBelle[1], Keith Yearby[2], and Jolene S. Pickett[3]

[1]Department of Physics and Astronomy, Dartmouth College, Hanover, NH, USA, [2]Department of Automatic Control and Systems Engineering, The University of Sheffield, Sheffield, UK, [3]Department of Physics and Astronomy, University of Iowa, Iowa City, IA, USA

Key Points:

- Similar or sometimes identical Auroral Kilometric Radiation (AKR) fine structure features are observed simultaneously at ground level and at >10RE geocentric distance
- Emitted power of escaping AKR features observed with spacecraft greatly exceeds that of simultaneous features observed at ground level
- The estimated footprint of the source field line of escaping AKR during the best correlated fine structure is close to the ground station

Correspondence to:
J. LaBelle,
james.w.labelle@dartmouth.edu

Citation:
LaBelle, J., Yearby, K., & Pickett, J. S. (2022). South Pole Station ground-based and Cluster satellite measurements of leaked and escaping Auroral Kilometric Radiation. *Journal of Geophysical Research: Space Physics*, *127*, e2021JA029399. https://doi.org/10.1029/2021JA029399

Received 30 APR 2021
Accepted 10 JAN 2022

Abstract Previous work suggests that Auroral Kilometric Radiation (AKR) leaks to low altitudes. To investigate this phenomenon, wideband wave measurements have been conducted simultaneously at South Pole, Antarctica, and at the Cluster satellites, during 35 intervals in 2018–2020. Leaked AKR is observed ~5% of the time at South Pole and escaping AKR ~31% of the time at Cluster satellites. Both types of AKR are composed of fine structure, and similar fine structure is often observed simultaneously in the AKR at the different locations. Around 0317 UT on 29 June 2020, identical features were observed simultaneously. Cluster interferometry shows that the footprint of the source field line during this event lies within a few hundred kilometers of South Pole. The estimated emitted power of the escaping AKR observed at Cluster in this event exceeds that of the leaked AKR observed at South Pole by many orders of magnitude, suggesting that mode conversion involved in generating leaked AKR is relatively inefficient. AKR fine structure which is identical at the two locations comprises ~0.1%–0.3% of AKR observed at Cluster when the South Pole receiver operates, and ~2% of AKR observed at South Pole when at least one Cluster satellite is tuned to the appropriate frequency range. The relatively low occurrence rates of coincident fine structure may be attributed partly to geometric and beaming considerations but also suggest that processes involved in generating leaked AKR at levels detectable at ground level have lower probability than those generating escaping AKR at levels detectable by distant spacecraft.

1. Introduction

One of the most significant discoveries in space physics in the 1970s was that the Earth is a radio planet; that is, the Earth's auroral zones emit intense radiation in the kilometric wavelength range called Auroral Kilometric Radiation (AKR) (Gurnett, 1974). These emissions are the terrestrial equivalent of intense decametric radiation from Jupiter, known since the 1950s (Burke & Franklin, 1955). The discovery of these emissions in the Earth's environment, where the physical conditions had been better determined with in situ measurements, enabled the generation mechanism, previously highly uncertain, to be fairly rapidly identified as the cyclotron maser instability (CMI) (Melrose, 1976; Wu & Lee, 1979). Since the 1970s, AKR wave modes, time variations, source regions, beam patterns, and fine structure features have become well described through hundreds of observations, and the theory has been refined, most notably since the FAST satellite mission established that AKR results from the CMI driven by a "horseshoe" electron distribution rather than a simple beam or loss cone distribution (Delory et al., 1998; Ergun et al., 1998, 2000; Pritchett et al., 1999).

Most of this previous work pertains to the dominant component of AKR, which is the escaping X-mode component. This mode with wave vectors initially perpendicular to the magnetic field is excited by the CMI in the deep density cavity associated with the auroral acceleration region, where the horseshoe distribution occurs, the plasma frequency is far smaller than the electron gyrofrequency ($f_{pe} << f_{ce}$), and the energetic plasma component characterized by the horseshoe distribution has density comparable to or larger than that of the background plasma (Ergun et al., 2000, and references therein). The excited X-mode waves are subsequently refracted by density structure outward in a beam aligned with the plane that is tangent to the magnetic field longitude at the source (Mutel et al., 2008). The emissions are sufficiently intense to be observed by satellites at great distances as long as they are within this beam pattern, and since at a given time there may be many AKR sources arrayed around the nightside auroral oval, AKR is commonly, sometimes almost continuously, observed with wave instruments

on the Cluster, Geotail, Polar, AMPTE/IRM, ISEE, and similar satellites. The outward beaming, together with the inability of X-mode at kilometric wavelengths to penetrate the ionosphere, explains why AKR was not discovered until the 1970s when suitably instrumented satellites were first launched into appropriately distant orbits, in contrast to the equivalent Jovian emissions which can be detected at ground level because their higher frequency penetrates the ionosphere (Burke & Franklin, 1955).

However, since shortly after its discovery, occasional observations have suggested that a component of AKR somehow penetrates to Low Earth Orbit (LEO) altitudes (LaBelle et al., 1999; Oya et al., 1985; Parrot & Berthelier, 2012; Shutte et al., 1997) or even ground level (LaBelle & Anderson, 2011; LaBelle et al., 1999, 2015). Oya et al. (1985), using the Ohzora (EXOS-C) satellite topside sounder in passive mode, observed many examples of waves with AKR-like structure at LEO altitudes, labeled these "leaked AKR" in contrast to the more intensely studied escaping X-mode AKR, and suggested a mechanism for them. LaBelle and Anderson (2011) observed simultaneously escaping AKR with the Geotail satellite at distances exceeding 100,000 km and leaked AKR measured at ground level, finding correlated features, suggesting that these phenomena are connected. Parrot and Berthelier (2012) observed AKR in low Earth orbit, in particular during a magnetic storm that shifted the auroral oval to latitudes covered by the DEMETER satellite. LaBelle et al. (2015) described further observations of leaked AKR at multiple observatories in Antarctica, showing that on occasion emissions were observed on up to four stations separated by >500 km, emissions were right-hand polarized with respect to the magnetic field as expected for whistler mode, and correlation between time variations of leaked AKR and those of escaping AKR observed with the Geotail satellite were weakly but not perfectly correlated, as expected since the distant satellite detected large numbers of AKR sources, not only those potentially illuminating particular Antarctic observatories, and on other occasions the sources illuminating the ground stations may have been out of view of the spacecraft due to the AKR tangent-plane beaming pattern. Establishing a connection between these phenomena through correlation alone is a challenging problem.

Starting shortly after the discovery of AKR, theory papers addressed possible mechanisms for leaked AKR. Jones (1976) put forth the second Ellis window as a mechanism to linearly convert Z-mode to whistler mode which can propagate to low altitude. Krasovskiy et al. (1983) proposed ballistic wave transformation whereby high-altitude AKR imprints the electron distribution which subsequently generates whistler mode signals at a lower altitude, and based on angular dependence and scaling arguments suggested that this mechanism could be more efficient than the usual linear transformation considered by Jones (1976). Chian et al. (1994) suggested that auroral Langmuir waves interact nonlinearly with Alfven waves may produce electromagnetic radiation in the AKR frequency range. Oya et al. (1985) further promoted the idea of mode conversion from Z-mode to whistler mode as the generation mechanism, parallel to a mechanism of O-mode AKR via mode conversion from Z-mode proposed by Oya and Morioka (1983). In this mechanism, conversion to whistler mode occurs either via linear transformation through the second Ellis window (Budden, 1988; Jones, 1976; Yoon et al., 1998), or via scattering on density gradients or irregularities or via nonlinear mechanisms.

Two theoretical approaches have considered excitation of Z-mode via CMI, in different regimes with different implications for observations. Wu et al. (1989), based on theory developed by Wu et al. (1983), consider parallel propagating modes excited by a few-keV ring distribution. They find instability peaking at $f \sim 0.8 f_{ce}$, and the growth rate decreases as f_{pe}/f_{ce} decreases from 0.8 to 0.2. Wu et al. (1989) state, "when these waves are propated downward along the magnetic field line, the resulting noise observed with a ground based facility will have a broad band in frequency." Ziebell et al. (1991) model the propagation and amplification of these modes, showing that the resulting radiation is broad band. (This broad band nature is inconsistent with the ground-level AKR observations shown in Figure 2 below, which are replete with narrow band fine structure, similar to that of escaping AKR.) Horne (1995) considers mode conversion and propagation to ground level. He finds that the waves can reach the second Ellis window and convert to whistler mode if the initial wave-vector is close to parallel to the magnetic field, within 0°–5° in one case studied and 5°–7° in another. The whistler modes subsequently propagate to ground level and illuminate a relatively narrow latitude range, around 2°. However his density model does not include horizontal gradients, which he acknowledges might allow waves with more perpendicular wave vectors to reach the Ellis window condition. Horne also finds that under conditions of extraordinarily low densities, for which $f_{pe} < f_{ce}$ throughout the ionosphere, the Z-modes can directly penetrate.

An alternative approach to CMI excitation of Z-mode was inspired by Cluster satellite observations of Z-mode in the auroral acceleration region in the direct vicinity of the X-mode AKR sources (Mutel et al., 2011). Figure 1

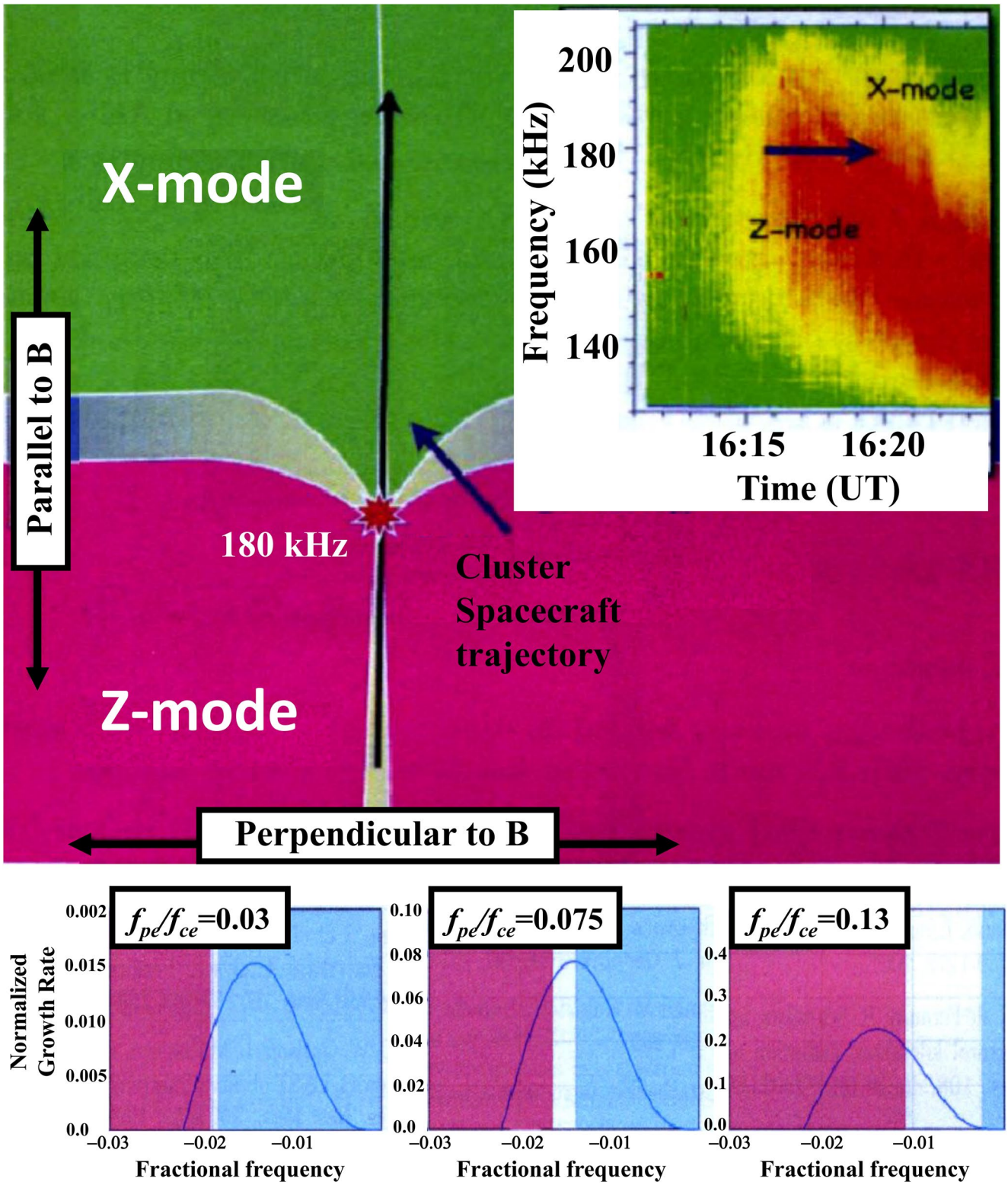

Figure 1. (Inset) Spectrogram of Auroral Kilometric Radiation (AKR) measured with the Cluster satellite as it traversed near a source region. (Upper panel) cartoon spatial dependence of the generation of X- and Z-mode AKR by the cyclotron maser instability (CMI) in a source region characterized by a downward pointing gradient of background density and a superposed deep field aligned density cavity. (Bottom panels) Calculated CMI growth rates assuming horseshoe electron distribution for three different f_{pe}/f_{ce} ratios, implying excitation of both X-mode (blue shade) and Z-mode (red shade). Adapted from Mutel et al. (2011). Reprinted by permission of Austrian Academy of Sciences Press.

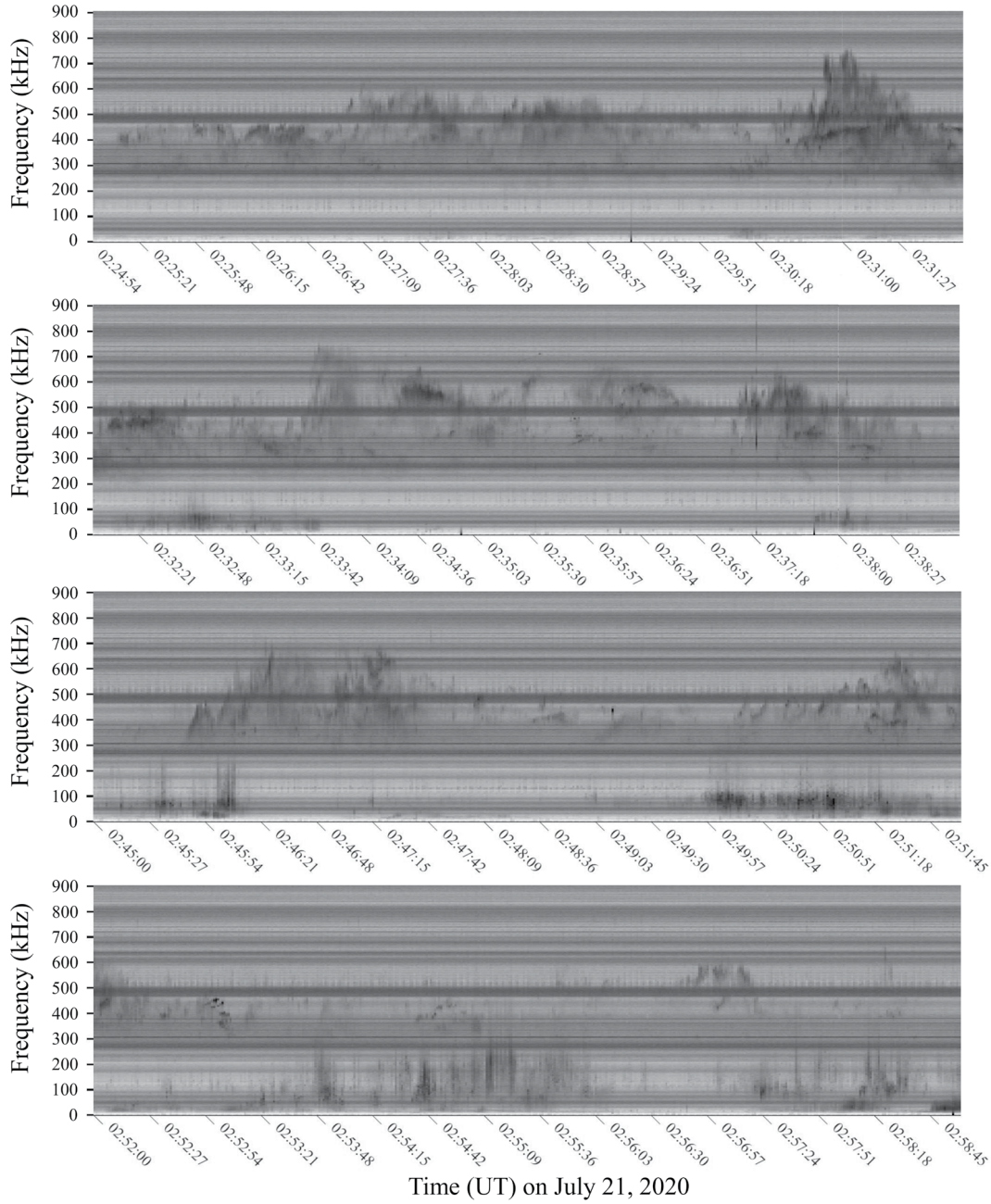

Figure 2. (Top panel) Spectrogram showing leaked Auroral Kilometric Radiation (AKR) measured at South Pole Station during four 7-min intervals on 21 July 2020; horizontal bands represent RF interference and should be ignored.

(inset), reprinted from Mutel et al. (2011), shows the direct observation of these Z-modes confirmed through the detection of a narrow null in the spectrum corresponding to the forbidden region in the wave spectrum between the Z- and X-modes. Mutel et al. (2011) also calculated CMI growth rates resulting from ~10 keV ring distribution, but considering wave vectors close to perpendicular to the magnetic field. They obtain instability for frequencies just below f_{ce} under conditions $f_{pe} << f_{ce}$, though for slightly higher f_{pe}/f_{ce} ratios than required for excitation of X-mode. These waves are therefore excited in the direct vicinity of the X-mode source rather than hundreds of kilometers lower (at $f \sim 0.8 f_{ce}$) as in the Wu et al. (1989) mechanism. Furthermore, Mutel et al. (2011) found that at a single location, CMI can excite both Z-mode and escaping X-mode depending on frequency. The bottom panels of Figure 1, reprinted from Mutel et al. (2011), show growth rate calculations for three values of f_{pe}/f_{ce}; in each case the waves are narrow band just below f_{ce}, with the lower part of this narrow band excited

in the Z-mode and the upper part in the X-mode, with X-mode (Z-mode) dominating more for smaller (larger) f_{pe}/f_{ce}. These calculations imply that not only will the resulting Z-mode radiation be narrow band similar to the X-mode, but that a particular sequence or evolution of electron distributions, giving rise to a particular complex fine structure pattern at an appropriate location within the source region, will generate fine structure features in X-mode and Z-mode that mirror each other. Both escaping and leaked AKR are characterized by fine structure, narrow bandwidth features that shift upward or downward in frequency with time in complex patterns (Gurnett & Anderson, 1981). These features can be as narrow as a few Hz (Baumback & Calvert, 1987) but more typically have 1–10 kHz bandwidths. Various patterns occur, only a few of which have attracted theoretical explanations (e.g., "striated AKR" Menietti et al., 2000; Mutel et al., 2006; Pottelette & Pickett, 2007). Finding even a few examples of these complex features exactly mirrored simultaneously in escaping X-mode and leaked AKR would be "smoking gun" evidence for a mechanism such as that described above linking these two phenomena.

Unfortunately, no study has yet undertaken the difficult task of modeling propagation and mode conversion of the oblique Z-mode waves excited at the AKR sources. Horne (1995), who focuses on parallel propagating modes predicted by Wu et al. (1989), finds that for a smooth density profile without horizontal density gradients, oblique Z-modes cannot reach the second Ellis window condition; however, the Z- and X-mode sources considered by Mutel et al. (2011) occur in a deep density trough associated with the auroral acceleration region, implying strong horizontal gradients. Alternatively, even if the oblique waves do not reach the Ellis window condition for linear conversion, non-linear conversion to whistler mode is a strong possibility in the inhomogeneous environment of the auroral acceleration region. Horne (1995) raises another possibility, that Z-mode may directly generate ground-level waves in extraordinarily low-density conditions in the ionosphere. The restriction of ground-level AKR to approximately 1 month either side of winter solstice (LaBelle et al., 2015) suggests a correlation with low densities. The International Reference Ionosphere (Bilitza et al., 2017) model for winter 2019 conditions do not indicate such low densities (maximum $f_{pe} < f_{ce}$) over South Pole; however, the ionosonde located at Jang Bogo Station (~1,000 km away) suggests this condition may occur on occasion in winter (top panel of Figure 7 of Ham et al., 2020). Propagation studies including full-wave treatment are required to understand the mechanisms by which oblique Z-mode wave generated in the auroral acceleration region can reach low altitudes or ground level. These studies are beyond the scope of this paper, but there clearly is no shortage of plausible mechanisms by which this can happen.

In summary, the narrow-band nature of "leaked AKR" shown in Figure 1 and the resemblance of its fine structure to that of escaping AKR make narrow-band Z-mode excitation in the acceleration region a more likely mechanism than excitation of parallel modes at lower altitudes which predicts broad band radiation. The connection between escaping X-mode and leaked AKR is challenging to prove experimentally. Even with a suitably instrumented satellite in the region where the mode conversion takes place, it would be challenging to observe the subtle differences in wave-vector distributions associated with a partial degree of mode conversion. Wave vectors and their distributions are notoriously difficult to measure in-situ. As mentioned above, seeking correlations has challenges because imperfect correlations are expected and observed. Simultaneous measurement of identical complex fine structure in escaping X-mode AKR and leaked AKR would, however, provide "smoking gun" evidence of a connection between these phenomena.

An experiment seeking this evidence requires high time- and frequency-resolution measurements of both the escaping X-mode AKR at great distances from Earth and the leaked AKR either in LEO or at the surface of the Earth. The latter are currently available from South Pole Station, continuously during austral winter and in the midnight magnetic local time sector. The former are available from the Cluster satellite wideband instrument on a much lower duty cycle. Unfortunately, the Geotail satellite plasma wave instrument, though available on a much higher duty cycle, has 8-s time resolution which does not sufficiently resolve AKR fine structure. Section 2 below reports results from initial experiments comparing South Pole and Cluster satellite wave data during 2018–2020. Section 3 discusses conclusions that can be drawn from these initial measurements.

2. Data Presentation

The receiving system used for most observations of leaked AKR at South Pole Station, Antarctica, consists of two approximately 40 m^2 wire loop antennas perpendicular to each other on a 30-foot mast, connected via approximately 1-km coaxial cable to a USRP model 200 two-channel digital receiver in the V-8 science vault

adjacent to the station. Low-noise preamplifiers at the base of the antenna convert induced current to voltage with impedance matched to the transmission line, and an interface box at the receiver end includes low-pass anti-alias filtering and high-pass filtering to prevent saturation by very low frequency (VLF) signals. The frequency response of the receiving system is approximately flat over the range 100–2,000 kHz. The receiver and associated computer are housed in an enclosure designed so that their combined energy dissipation keeps them at an optimal operating temperature. The computer is connected to the internet, allowing control of the experiment from Dartmouth College. Data are stored primarily on a second computer in the B-2 science lab in the station. For the experiments reported herein, the receiver was operated in one of two modes: "continuous mode," in which complex I and Q signals are sampled continuously at 2 MHz with 1 MHz center frequency, typically for five hours each day (00–05 UT, where 0350 UT is local magnetic midnight at South Pole); and "synoptic mode," in which 25k samples of each channel (at 2 MHz sample rate and 1 MHz center frequency) are retained each one second. Continuous mode, required to measure AKR fine structure, results in >260 GB/day, so that a scientist in the loop must inspect the data approximately weekly, discarding uninteresting time intervals. This procedure results in 5–6 TB of data during an austral winter. A second receiving system consisting of 10 m^2 loop antennas, artificially injected reference and calibration signals, analog filtering/automatic gain control, and 10–20 MHz analog-to-digital conversion, is less sensitive but contributes to calibration and accurate time synchronization of the AKR measurements. These systems were designed, built and tested at Dartmouth College and installed at South Pole Station by Dartmouth College personnel. They were operated during austral winters of 2018, 2019, and 2020.

The four Cluster spacecraft are in elliptical polar orbits with perigee currently around 5 R_E and apogee 16 R_E. During AKR observations the inter-spacecraft separations range from 2000 km to more than 12,000 km, with a positional accuracy of around 1 km. The spacecraft are spin stabilized at 15 RPM, and each has a pair of 88 m tip-to-tip wire boom electric field antennae orientated in the spin plane. Only one antenna may be connected to the Wideband Data receiver at one time, so it is not possible to make measurements of wave polarization with this receiver. The Wideband Data (WBD) experiment (Gurnett et al., 1997), mounted on all four Cluster spacecraft, provides high-resolution waveform measurements of a single electric field component up to 577 kHz. Frequencies above 77 kHz are handled in a translation mode whereby a selected frequency band is down-converted to baseband. Three translation bands of 125, 250, and 500 kHz are normally used in sequence to allow a wide range of frequencies to be sampled. The waveform is sampled using an 8 bit analog to digital converter with automatic gain control to provide a dynamic range up to 120 dB. In Burst Mode 2, which is used for the data presented herein, data may be acquired in a wide band (77 kHz) duty cycled mode or narrow band (4.2 kHz) continuously sampled mode. Telemetry is recorded onboard at 73 kbit s^{-1} for later downlink to a ground station. (The experiment also has a 220 kbit s^{-1} real time telemetry mode, but this is not used for the current work.) The University of Iowa and University of Sheffield were involved in design, construction, testing, and post-launch operation and data acquisition for the Cluster WBD experiment.

Figure 2 shows 0–900 kHz spectrograms showing leaked AKR detected with the South Pole experiment described above during selected seven-minute intervals on 21 July 2020. Horizontal bands in the spectrograms represent artificial interference and should be ignored. For these spectrograms and all South Pole data subsequently used in this study, the signals from the crossed antennas have been recombined, producing the effect of an antenna rotated 29° between them, which resulted in the cleanest possible spectra in the 500–600 kHz frequency band by causing the greatest degree of cancellation of the artificial interference. The AKR in this example extends from 200 to 750 kHz and exhibits complex fine structure, strongly resembling fine structure of escaping X-mode AKR observed with spacecraft (e.g., Gurnett & Anderson, 1981). Also visible is auroral hiss, including VLF hiss below 30 kHz strongly suppressed by the instrumental high-pass filter and various types of LF hiss extending to hundreds of kHz. LF hiss shares the same frequency range as leaked AKR but appears entirely different on frequency-time spectrograms, as pointed out by LaBelle et al. (2015).

As mentioned above, operations of the wideband instrument on the Cluster spacecraft were limited to 10–16 two- to four-hour intervals during each of the three austral winters of this experiment (2018–2020). The South Pole receiver was operated in continuous mode during nearly all of these intervals. Table 1 summarizes intervals during which observations were made at each location, also showing the average locations of the Cluster satellites during each conjunction. The center columns of Table 1 indicate whether AKR was detected by the receivers at any time during the interval (though in some cases not simultaneously). In 2018, intervals were assigned ahead of time during austral winter times when South Pole was in the midnight magnetic time sector and Cluster was at the

Table 1
Summary of South Pole and Cluster Coordinated Auroral Kilometric Radiation (AKR) Observations and AKR Occurrence Rates

				Cluster spacecraft position		
Date and time range		AKR at SP	AKR at Cluster	λ_m	MLT	R
2018-06-09 01:00	2018-06-09 05:00	0%	27%	−55.3	10.4	11.3
2018-06-18 02:30	2018-06-18 05:00	0%	8%	−57.8	10.5	10.9
2018-07-06 02:00	2018-07-06 04:30	1%	58%	−55.2	11.2	8.2
2018-07-13 00:00	2018-07-13 04:00	0%	51%	−55.2	7.8	11.2
2018-07-31 01:00	2018-07-31 05:00	3%	37%	−54.7	7.5	10.1
2018-08-09 01:00	2018-08-09 05:00	0%	24%	−53.0	8.2	9.2
2018-08-18 02:00	2018-08-18 06:00	0%	29%	−49.6	7.8	8.9
2019-05-27 22:50	2019-05-28 01:50	0%	41%	−51.0	11.1	11.7
2019-05-29 23:40	2019-05-30 02:40	0%	89%	−52.7	12.9	8.5
2019-06-05 23:50	2019-06-06 02:50	21%	16%	−53.3	10.3	11.6
2019-06-08 00:40	2019-06-08 03:40	1%	22%	−55.4	11.9	8.6
2019-06-15 00:40	2019-06-15 03:40	0%	41%	−54.4	9.5	11.5
2019-06-24 01:30	2019-06-24 04:30	5%	31%	−54.1	8.7	11.3
2019-07-03 00:00	2019-07-03 03:00	0%	2%	−56.0	10.5	9.9
2019-07-12 01:00	2019-07-12 04:00	32%	15%	−56.5	9.6	9.8
2019-07-19 01:30	2019-07-19 04:30	20%	51%	−42.5	5.4	12.8
2019-07-21 01:30	2019-07-21 04:30	36%	66%	−49.3	6.2	10.3
2019-07-28 00:40	2019-07-28 03:40	0%	29%	−49.1	5.6	11.9
2019-08-08 01:40	2019-08-08 04:40	0%	34%	−52.6	6.4	8.8
2020-05-10 01:45	2020-05-10 03:15	0%	0%	−46.4	15.6	7.5
2020-05-17 00:00	2020-05-17 01:30	0%	6%	−48.8	11.8	10.0
2020-05-19 02:50	2020-05-19 04:20	0%	36%	−50.1	15.0	7.4
2020-05-28 02:30	2020-05-28 04:00	0%	0%	−37.2	16.1	6.6
2020-06-03 23:15	2020-06-04 00:45	31%	51%	−47.3	13.5	7.8
2020-06-06 03:30	2020-06-06 05:00	0%	11%	−39.5	15.5	6.5
2020-06-11 02:00	2020-06-11 04:00	0%	49%	−33.9	7.2	13.3
2020-06-13 00:30	2020-06-13 02:00	0%	0%	−52.1	12.5	7.9
2020-06-20 02:30	2020-06-20 04:30	0%	7%	−33.6	6.7	13.0
2020-06-29 02:00	2020-06-29 04:00	7%	49%	−38.8	6.5	12.0
2020-07-05 23:30	2020-07-06 01:30	0%	18%	−33.3	5.6	13.6
2020-07-08 02:30	2020-07-08 04:30	8%	37%	−38.5	6.0	11.7
2020-07-15 00:00	2020-07-15 02:00	6%	51%	−33.3	5.0	13.2
2020-07-17 03:00	2020-07-17 05:00	0%	14%	−38.3	5.5	11.3

Table 1
Continued

Date and time range		AKR at SP	AKR at Cluster	Cluster spacecraft position		
				λ_m	MLT	R
2020-07-24 00:30	2020-07-24 02:30	16%	79%	−32.9	4.4	12.9
2020-07-26 03:00	2020-07-26 05:00	0%	44%	−41.3	5.4	10.5
Average		5%	31%			

Note. The tabulated Cluster spacecraft position is the average of all spacecraft included in the observation, averaged over the duration of the interval, defined by magnetic latitude (l_m), magnetic local time (MLT), and geocentric radial distance (R). The percentage AKR observed at South Pole is the number of minutes during which AKR was observed divided by the total number of minutes observation. The percentage AKR observed by Cluster is the proportion of spectra where the wave intensity exceeds a threshold approximately 5 dB above the receiver noise level (only AKR is observed at this location and frequency range, it being well above the local electron cyclotron frequency and plasma frequency).

high latitudes needed to observe southern hemisphere AKR. In subsequent years, interval selection was guided by progressively better information about occurrence rates at South Pole and by application of the tangent plane beaming model (Mutel et al., 2008) to select times when AKR sources on field lines connected to South Pole could illuminate the Cluster satellites. As a result, the fraction of intervals in which AKR was observed at both locations significantly increased, to about 40% of the intervals in 2019–2020. Overall, during these observations, AKR was observed 5% of the time at South Pole and 31% of the time on Cluster.

Figure 3 shows the only example of AKR observed at both locations during the 2018 austral winter. The top panel is a 500–625 kHz spectrogram of South Pole data showing two brief bursts of AKR starting at 0138:10 and 0138:30 UT on 31 July 2018. Horizontal bands of noise below 520 kHz and above 590 kHz are radio frequency interference and should be ignored. As mentioned above, the Cluster satellites sample different frequency ranges in sequence, dwelling for approximately one minute on each range. This method allows a wide range of frequencies to be sampled within the constraints of the satellite resources, but sometimes results in missing coincident events as happens in this case. The bottom panel of Figure 3 is a 500–625 kHz spectrogram of Cluster-C2 satellite data showing intermittent AKR during the 50-s interval, 0137:29–0138:16 UT, when the Cluster wideband receiver dwelt on this frequency range. The apparent decrease of wave power above 600 kHz is due to the instrumental low-pass filter and should be ignored. AKR commences in both records in the same frequency range, 510–550 kHz, at the same time, 0138:10 UT. For the approximately 7 s of simultaneous measurement, the appearance of the AKR in the frequency-time diagrams is remarkably similar. At this time, Cluster was located at $\lambda_m = -57.03$, MLT = 9.5, at a geocentric distance of 8.25 R_E (12,976, −11,008, and −49,742 km in GSE coordinates). This example of coincident AKR fine structure in escaping X-mode and leaked AKR across such a large separation distance is intriguing, but the short duration of the overlapping measurements limits how conclusive the observation is.

Figure 4 shows 502–582 kHz spectrograms covering 140 min on 6 June 2019, an interval during which bursts of AKR occurred simultaneously at South Pole and Cluster C4. The Cluster C4 data in this frequency range were recorded with 50% duty cycle during this time interval; line features in both data sets are due to interference and should be ignored. Bursts of AKR occur at both locations during 2350–0000 and 0042–0044 UT. At other times bursts are observed at one location but not the other, more often at Cluster than at South Pole, consistent with the overall occurrence rates summarized in Table 1. Figure 5 shows an expanded view of the coincident AKR observed near 0042 UT in Figure 4. Top and bottom panels show 510–610 kHz spectrograms from the South Pole and Cluster C4 receivers, respectively, during 0041:21–0043:01 UT. Narrow horizontal lines in the South Pole spectra as well as broader noise bands near 500 and 600 kHz are due to interference and should be ignored; the decrease in power spectral density above about 585 kHz in the Cluster C4 data is due to instrumental low-pass filter and should be ignored. At this time, Cluster was located at $\lambda_m = -54.2$, MLT = 10.8, at a geocentric distance of 11.3 R_E (20,199, −30,565, and −62,119 km in GSE coordinates). At both locations the primary AKR observed during this time occurs during the same one-minute interval, 0041:58-0042:58, and the AKR is similarly broadband at both stations, mostly covering the entire range measured (500–610 kHz in the case of South Pole; 500–580 kHz in the case of Cluster C4); the fine structure appears as mainly vertically oriented features, at times perhaps rising tones, on both frequency-time spectrograms. In particular, vertical features near 0042:20 appear coincident; vertical features at 0042:00–0042:05 UT

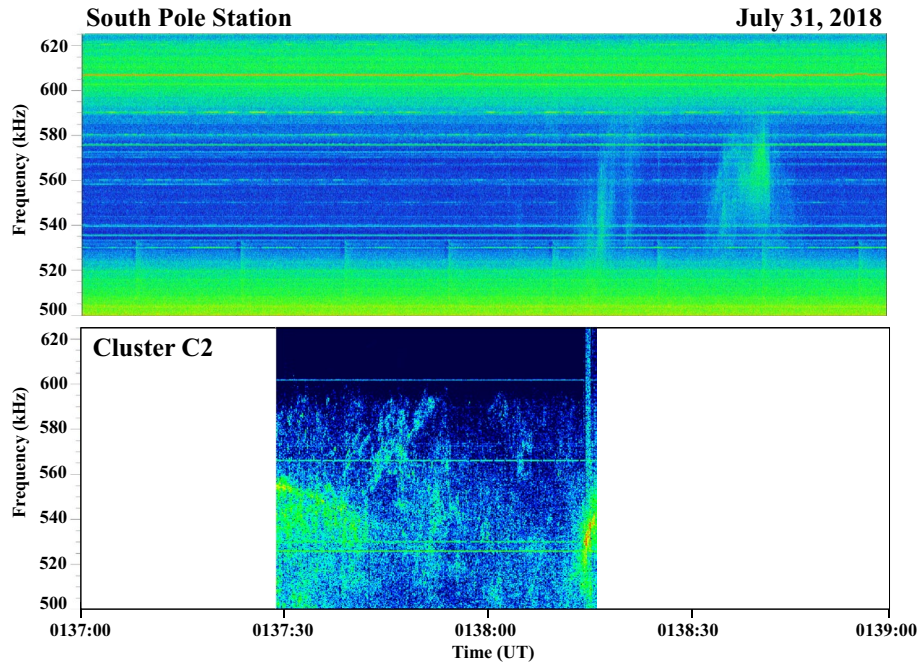

Figure 3. 500–625 kHz spectrograms of leaked Auroral Kilometric Radiation (AKR) observed at South Pole (top panel) and escaping AKR observed with the Cluster C2 satellite (bottom panel).

less so. At both locations, sporadic bursts of AKR occur prior to 0042 UT. This example shows resemblance between simultaneous escaping X-mode AKR at Cluster and leaked AKR at South Pole, though the absence of discrete fine structure features makes it inconclusive whether the exact same sources are responsible.

Figure 6 shows another example of AKR observed at both locations during a 100-s interval, 0338:30–0340:10 UT on 21 July 2019, in similar format as Figure 5. At least two significant AKR features are visible in the South Pole data: two short impulsive rising tones covering 510–550 kHz and 510–580 kHz at 0338:54/0338:56 UT, and a dramatic arch-like feature emerging from below 500 kHz at 0339:30 UT, reaching a maximum frequency of 580 kHz at 0339:42 kHz, and descending below 500 kHz at 0340 UT. AKR occurs almost throughout this 100-s interval in the Cluster-C2 data, but interestingly it includes an arch-like feature similar to that seen in the South Pole data, emerging from below 500 kHz at 0339 UT, reaching a maximum frequency of 580 kHz at 0339:25 UT, and descending below 500 kHz at 0339:52 UT. These arch-like features are not simultaneous, so they presumably do not result from the exact same source location. However, the identical frequency ranges suggest sources at nearly the same altitude. The similarity in form and frequency range of these arch-like features indicates that whatever complex evolution of the electron distribution function is required to explain such an arch feature is occurring at each source, suggesting they are within the same evolving electron beam.

Figure 7 shows an example of AKR observed at both locations during the 2020 austral winter. In this case, 2–1/2 min of data are displayed, 0316:30–0319:00 UT on 29 June 2020. South Pole data are in the bottom panel, and the top panel shows data from two different Cluster spacecraft: C4 during the first 50-s interval, C1 during the middle 50-s interval, and C4 during the third 50-s interval. As in Figures 3–6, interference lines in the South Pole data and the instrumental roll-off above 585 kHz in the Cluster satellite data should be ignored. The South Pole receiver was in synoptic mode during most of the interval, except for 0316:57–0317:57 UT when it was in continuous mode with better time resolution. At this time, the Cluster satellites C1 and C4 were close to each other, with C1 at 12.1 R_E, −33.5 MLAT and 6.3 MLT. The South Pole receiver detects leaked AKR for about 45 s, 0316:55–0317:40. It consists of an ascending frequency feature of initially about 10 kHz bandwidth, followed by a descending frequency feature of somewhat broader bandwidth. The Cluster wideband receivers detect AKR throughout the time interval. However, most striking in the Cluster C4 data is an ascending frequency feature of about 10 kHz bandwidth starting at 0316:55 UT, coinciding exactly in both time and frequency with the ascending frequency feature simultaneously observed at South Pole. A descending frequency feature following

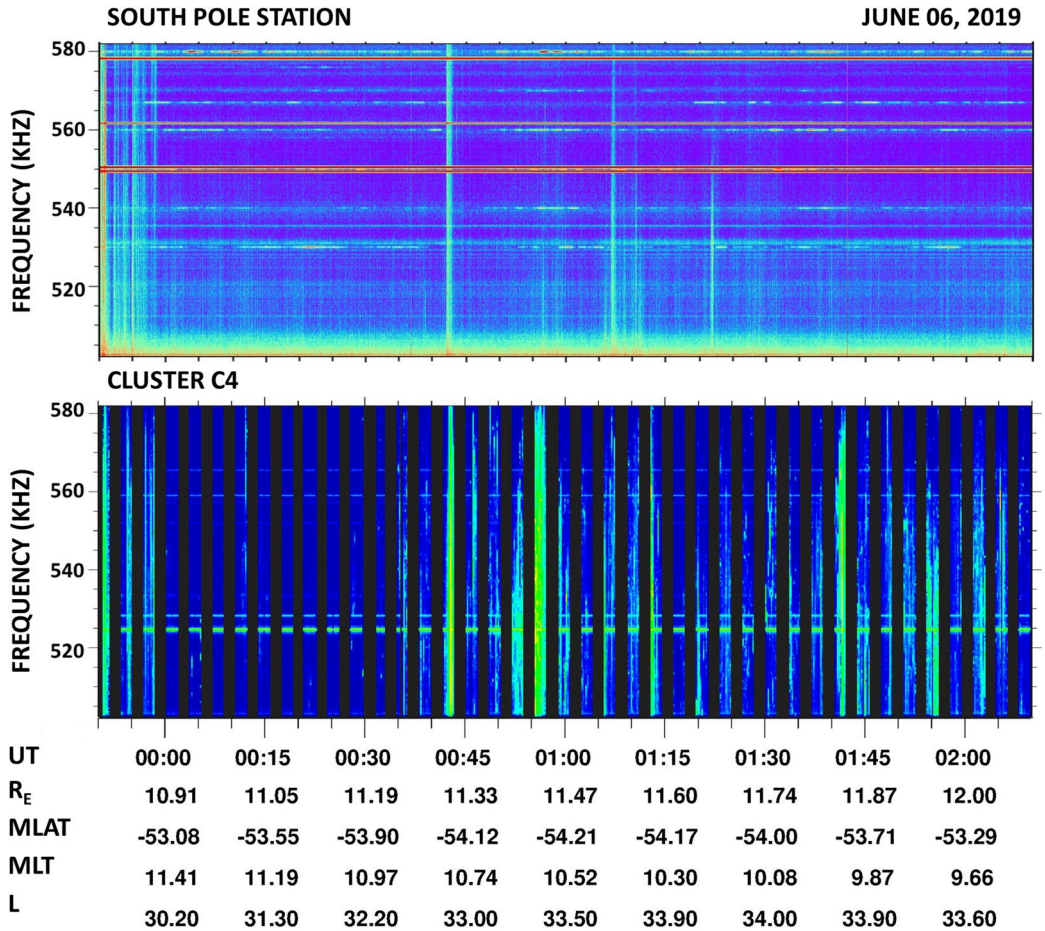

Figure 4. 502–582 kHz spectrograms of leaked Auroral Kilometric Radiation (AKR) observed at South Pole (top panel) and escaping AKR observed with the Cluster C4 satellite (bottom panel), showing intervals of coincident occurrences.

this appears in the Cluster C1 data, similar to but not as closely resembling the simultaneous descending feature observed in the South Pole data.

Two analyses were conducted to more quantitatively assess the correlation between the ascending frequency features seen simultaneously in the Cluster C4 and South Pole data. This assessment is challenging because the Cluster satellites clearly detect more AKR sources than are observed at South Pole. First, South Pole power spectral densities were re-binned to the same frequency and time resolution of the Cluster C4 data, and the Pearson correlation coefficient was computed to compare them. Averaging over 857 Hz in frequency and approximately 2 s in time to avoid issues with spin modulation of the Cluster data, the result is a correlation of 0.44, which is robust to slight shifts in time or frequency. Randomly permuting the original data sets and re-computing the correlation coefficient yields values below 0.16 every time in a sample of 10^4, suggesting that values of 0.44 and above are unlikely to occur by chance at a confidence level of at least 10^{-4}. Both the constraint on this conclusion and the relatively low correlation coefficient result because the satellite detects additional sources not observed at South Pole. As a complementary test attempting to account for this effect, a peak-tracking algorithm was applied to each data set, at each time step identifying the highest maximum of power spectral density within 10 kHz of the average of the previous five peaks, resulting in time series of peak frequencies tracing out the ascending feature observed in the two datasets between 6 and 15 s after 0317 UT. Fitting each series of peak frequencies to a line yielded slopes of 3.60 ± 0.11 kHz/s for the South Pole spectra and 3.44 ± 0.25 kHz/s for the Cluster satellite spectra. The former slope lying well within 1-sigma of the latter is another strong indicator that the signals are correlated better than by chance.

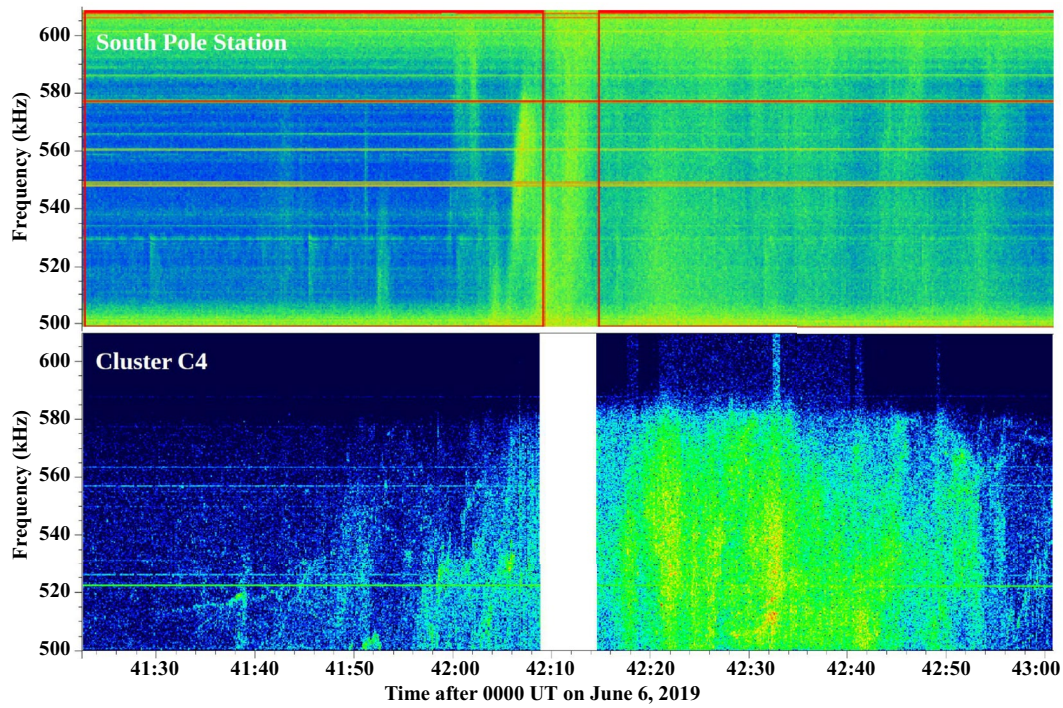

Figure 5. 500–610 kHz spectrograms of leaked Auroral Kilometric Radiation (AKR) observed at South Pole (top panel) and escaping AKR observed with the Cluster C4 satellite (bottom panel).

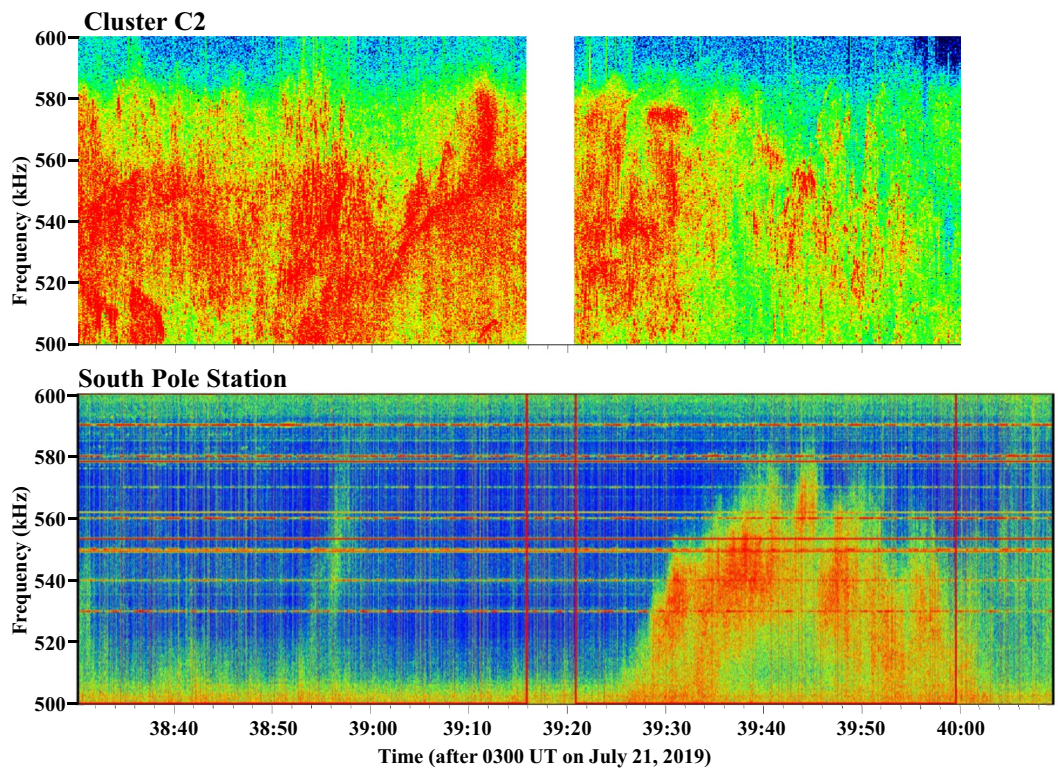

Figure 6. 500–600 kHz spectrograms of escaping Auroral Kilometric Radiation observed with the Cluster C2 satellite.

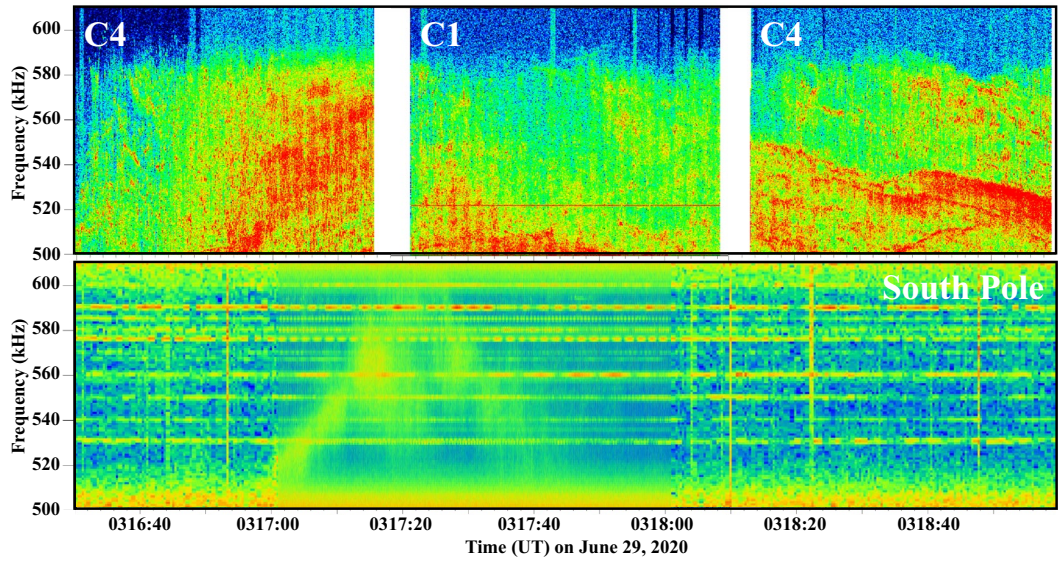

Figure 7. 500–610 kHz spectrograms of escaping Auroral Kilometric Radiation observed with the Cluster C1 and C4.

Although they last only 20–45 s, these coincident features, especially the simultaneous ascending frequency features, are the best candidate example yet observed for which the spacecraft and ground station, separated by 10 R_E, may be observing escaping X-mode and leaked AKR from the same source. The event is fleeting: when C4 next dwells on the 500–600 kHz band, starting at 0318:13 UT, strong structured AKR is still ongoing at the C4 location, but there is no leaked AKR visible above the noise level at South Pole.

As Table 1 shows, AKR at South Pole Station and at least one Cluster satellite occurred during conjunctions on five other dates in 2020 besides June 29, as well as other intervals on June 29 besides that shown in Figure 7. In many examples some degree of correlation exists between the signals at the two locations, similar to Figure 5, In many other examples structured leaked AKR observed at South Pole unfortunately coincides with intervals when the Cluster wideband receiver was tuned to different frequency ranges, and in other examples structured AKR at one or the other location corresponds to absence of AKR at the other location, or to structured AKR with no correlation between the structures. All of these outcomes are not surprising, considering the vast distance between the observing locations, and that the Cluster satellites can detect AKR from a wide range of locations around the auroral oval, not just those connected to South Pole. Even between the relatively closely spaced Cluster satellites themselves, AKR fine structure often differs. Mutel et al. (2003) determined the source locations of individual AKR bursts using cross-correlation of AKR waveforms received on the four Cluster satellites. Spacecraft separations varied up to 12,000 km (about 10° in angle viewed from the source), yet even on this scale only around 4% of data windows with detectable AKR emission produced valid solutions. This is attributed to multiple sources contributing to the AKR detected in each window.

3. Discussion

As discussed in the introduction, simultaneous observation of identical fine structure in escaping and leaked AKR comprises strong evidence for a direct connection between those phenomena, such as simultaneous excitation of X- and Z-modes by the cyclotron maser mechanism followed by mode conversion and propagation of the latter to low altitudes. While electron beams generating X-mode AKR could also generate whistler mode at lower altitudes, this process would not produce a match between the wave frequency and structure: the AKR frequency equals the electron gyrofrequency at its source altitude, but this frequency corresponds to an arbitrary frequency below the gyrofrequency at lower altitudes, where whistler mode auroral hiss is typically generated with entirely different frequency structure (examples shown in LaBelle et al., 2015). Therefore, the short interval near 0317 UT on 29 June 2020, provides the best evidence yet of AKR fine structure possibly generated simultaneously at a single location into escaping X-mode and trapped Z-mode converting into whistler mode, resulting in a fine structure feature, in this case an ascending frequency with ~10-kHz bandwidth, observed simultaneously in space

and at ground level. Short intervals on 31 July 2018 and 6 June 2019, provide weaker evidence of the same effect. These few cases cannot be considered conclusive, but they suggest a connection between escaping X-mode and leaked AKR, and they demonstrate the power of this experimental method to provide convincing proof through more examples.

Interestingly, all of the leaked AKR examples in this paper occurred in winter generally within 1 month of solstice. Previously reported examples also occurred during winter (e.g., Table 1 of LaBelle et al., 2015). Several satellite studies have shown a marked seasonal dependence whereby the AKR source region extends to lower altitudes in the winter hemisphere than in the summer hemisphere (Green et al., 2004; Kumamoto et al., 2003). Lower altitude sources could present a more favorable condition for propagation of mode converted AKR to low altitudes. Similarly, the relatively high frequencies of the leaked AKR in these examples, 500–600 kHz, correspond to relatively low altitude sources in the range 2,500–3,000 km.

A comparison of the amplitudes of the signals potentially sets constraints on the mode conversion process involved in generation of leaked AKR. The average root power spectral density of the ascending frequency feature detected at South Pole just after 0317 UT on 29 June 2020, is about 40 nV/m$\sqrt{\text{Hz}}$, implying 4×10^{-18} W/m^{2}Hz. Multiplying by the 10 kHz bandwidth implies an rms signal level of 4 μV/m and energy flux 4×10^{-14} W/m^2. The area illuminated by the leaked AKR is highly uncertain, but LaBelle et al. (2015) show examples simultaneously observed at Antarctic stations separated by as much as 1,143 km. This spreading of the energy may be primarily explained by sub-ionospheric propagation, but taking 1000 km as the diameter of the illuminated region implies an upper bound for the total power for this leaked AKR feature at ground level of 35 mW. At Cluster C4, the power spectral density of the simultaneous ascending frequency feature at the same time is approximately 10^{-12} V^2/m^{2}Hz, implying 3×10^{-15} W/m^{2}Hz; multiplying by the bandwidth implies 3×10^{-11} W/m^2. Cluster is at 12.5 R_E, or about 11.7 R_E from the source; assuming emission into a 20-degree wide beam about the tangent plane into the outward half-space equals approximately one steradian which at 11.7 R_E implies 5.6×10^{15} m^2, an upper bound on the area illuminated at the distance of Cluster C4. The resulting total power for this escaping AKR feature is 170 kW. Although both estimates are highly uncertain upper limits, they together suggest that the leaked AKR component at ground level is much lower power than the escaping X-mode component by a factor of order 2×10^{-7}.

The growth rate calculations and in situ Cluster observations of X- and Z-mode generation by the CMI mechanism in the auroral acceleration region suggest that these modes are produced with comparable amplitudes. Therefore, if the mode conversion of the Z-mode is responsible for leaked AKR, the observed ratio of leaked to escaping AKR power implies that the mode conversion must be relatively inefficient. In particular, it is unlikely that the bulk of the Z-mode wave power, emitted with wave vector perpendicular to the magnetic field, refracts on the density gradients to the Ellis window condition, since this would imply efficient mode conversion, and with the converted waves parallel to the magnetic field implying they are also likely to be transmitted efficiently through the Earth-ionosphere boundary. This scenario is unlikely in any case, since the required refraction is extreme and the refraction of the Z-mode in the conditions in the auroral cavity would be outward rather than downward on the background gradients. The observed low power ratio suggests that a less efficient mode conversion mechanism is likely; for example, scattering on a sharp density gradient or irregularity would convert a small portion of the Z-mode energy into whistler modes with a wide angular range, with only those within a few degrees of parallel having a chance to penetrate the Earth-ionosphere boundary.

As mentioned in the previous section, the "hit rate" of coincident AKR events increased significantly between 2018 and 2019–2020 when tangent plane beaming was taken into account in planning the conjunction times. This fact by itself provides further evidence of the tangent plane beaming model (Mutel et al., 2008). Figure 8a shows the foot print of the estimated location of AKR sources determined by differential time delay measurements (Mutel et al., 2003) at the four satellites during six selected 2020 conjunctions (also listed in Table 1), and for frequency 500 kHz. At any given time, Cluster can detect AKR occurring over a wide region. Interestingly, the date of the noteworthy correlation of fine structure between Cluster and South Pole, June 29, corresponds to a wide range of source locations which of all the selected dates overlaps most closely with the location of South Pole, indicated by a black square in Figure 8a. Further, Figure 8b shows the footprint geographic latitude as a function of time for the observations of June 29. (The measurements are bunched into columns because the source location estimates can only be done during the roughly one minute in four when the receivers operate in narrow band mode.) The footprints with most southerly latitude occur just around the time of the fine structure correlation. Keograms of

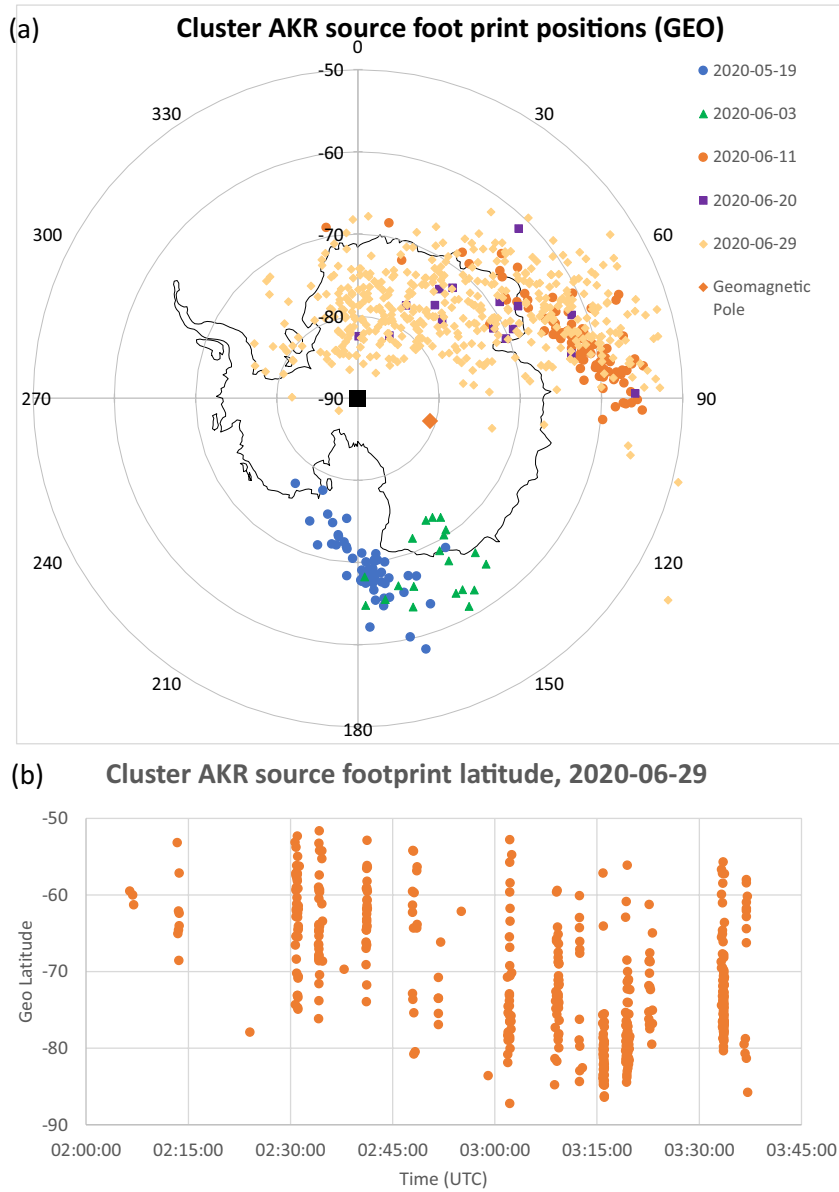

Figure 8. (a) Polar plot of footprints of Auroral Kilometric Radiation source locations observed by the Cluster satellites during selected conjunction intervals. (b) Footprint latitude versus time for conjunction on 29 June 2020. The best fine structure correlation was observed on this day at 03:17, which is just at the time of the most southerly latitudes.

South Pole all-sky camera data show aurora on the equatorward horizon at the time of the June 29 correlated AKR event, which is consistent with the source locations inferred from Cluster interferometry. (Keogram data corresponding to events shown in Figures 3 and 5 also show aurora equatorward; keogram data corresponding to the event shown in Figure 6 shows no aurora in view but the daily pattern suggests equatorward aurora, as is typical at South Pole for magnetic local times in the midnight sector.) This evidence supports the notion that the satellite and ground station would more likely observe the same source near 0317 UT on June 29. Of course, it is not essential that the source locations overlap with the ground station, since whistler mode signals can propagate significant distances sub-ionospherically after they penetrate the Earth-ionosphere boundary, and also it is unknown how much the energy spreads out in propagating from the source altitude to the ionosphere.

During 2018–2020, 37% (13 of 35) of the planned Cluster conjunction intervals overlapped with at least some leaked AKR detected above the noise level of the South Pole receiving system. The total duration of these conjunction intervals was 89.5 hr. The total duration of leaked AKR within these intervals was 287 min, implying

a leaked AKR occurrence rate of 5.3% during the conjunction intervals, which should be considered an upper bound on the occurrence rates because intervals of intermittent AKR were counted within the 287 min.

Within this time, approximately 1–2 min of exactly correlated fine structures occurred, as shown in Figures 3–7. A meaningful metric is the fraction of time that the Cluster sees AKR, for which correlated AKR is seen at South Pole Station. For approximately 1/3 to 1/2 of the conjunction intervals, Cluster was tuned to the incorrect frequency range to detect the South Pole AKR, and furthermore AKR occurred at Cluster during 31% of the conjunction intervals (Table 1); the fraction of Cluster AKR fine structure closely correlated with that at South Pole is therefore of the order of 0.1%–0.3%. Two possible sources of this low probability are: low probability of processes required to produce leaked AKR from any particular source of escaping X-mode AKR, namely the mode conversion at high altitudes and transmission through the Earth-ionosphere boundary at low altitudes; and a relatively small area on the ground typically illuminated by a given leaked AKR source. If the source of AKR observed at Cluster at an arbitrary moment is equally likely to originate anywhere on the nightside between 65 and 75 magnetic latitude, an area of 20×10^6 km^2, then explaining the occurrence rate as entirely due to geometry would require that the area illuminated on the ground have a radius of ∼150 km, which seems inconsistent with considerations of sub-ionospheric propagation and with LaBelle et al. (2015) observations of leaked AKR over hundreds of km baselines. Furthermore, this is probably an upper bound by a significant factor since in two of the three years, the Cluster conjunction intervals were selected to be times when the South Pole field line is more likely to be within the Cluster field of view according to the tangent plane beaming model, and the difference between numbers of events in 2019–2020 versus 2018 suggest that this selection was effective. Therefore, the probability of the chain of events required for leaked AKR to produce observable amplitudes at South Pole probably also plays a significant role in explaining the low occurrence rate.

Another consideration is the fraction of leaked AKR fine structure observed at South Pole which is simultaneous with escaping AKR fine structure observed with the Cluster satellites. For this consideration, the 287 min of ground-level leaked AKR observed during the conjunctions should be reduced by about a factor two because intervals of intermittent leaked AKR were counted, and by another approximately factor two because Cluster was measuring a different frequency range for that fraction of the time. The resulting fraction is about 2% (1–2 min out of 287/4 min). Geometry may play a larger role explaining this ratio; for the upper bound of illuminated area used in the power calculations above, tangent plane beaming covers about 1 steradian or perhaps 10% of the sky, and since this is an upper bound, it could explain the observed 2% fraction. However, as mentioned above, in two of the 3 years the conjunction orbits were selected to maximize probability that Cluster was within the region illuminated by sources on the South Pole magnetic field line, apparently with some degree of effectiveness, which implies that geometric factors alone may not explain the small percentage. Another factor may be the requirement that in order to be detected with the Cluster satellite, individual sources must stand out among the large number of sources within the satellite field of view. A full explanation of the small fraction of South Pole leaked AKR fine structure detected on the Cluster satellites requires better theoretical and experimental understanding of these phenomena.

4. Conclusions

In summary, simultaneous wideband wave observations of leaked AKR measured at South Pole Station and escaping AKR measured at the locations of the Cluster satellites show that qualitatively similar fine frequency structures often occur simultaneously at these two locations, and on rarer occasions identical features occur simultaneously. During the latter type of observation on 29 June 2020, Cluster satellite interferometry indicates that the footprint of the source field line for the escaping AKR lies within a few hundred kilometers of South Pole, and the estimated ratio of total power in the escaping AKR fine structure feature to that in the leaked AKR exceeds 10^6, suggesting that mode conversions relating these two phenomena need not be very efficient. Based on the limited statistics available in this study, coinciding identical fine structure features are relatively rare, occurring in about 0.1%–0.3% of AKR observed at Cluster and about 2% of leaked AKR observed at South Pole. There are ample reasons to understand why such events should be rare, including geometrical/spatial sampling considerations as well as the probabilities of processes leading to occurrence of leaked AKR at detectable levels at ground level. Of several mechanisms for leaked AKR discussed in the literature, these observations favor CMI excitation of Z-mode near f_{ce} in the auroral acceleration region in close vicinity to the sources of escaping X-mode AKR, as opposed to alternative mechanisms which generate broad band radiation not directly connected to the

X-mode excitation. Work beyond the scope of this paper is required to prove that oblique Z-mode waves excited in the auroral acceleration region can reach ground level, but a host of plausible mechanisms exist, such as linear or nonlinear conversion to whistler modes. The few cases of exactly matching fine structures observed so far do not comprise conclusive proof of the direct connection between escaping and leaked AKR, but they suggest such a connection, place constraints on those processes, and show the promise that continued coincident observations of these phenomena may better establish the connections between them.

Conflict of Interest

The authors declare no conflicts of interest relevant to this study.

Data Availability Statement

Data used in this study are available through LaBelle (2022). The Cluster WBD waveform data and location data used in this study are available at the Cluster Science Archive, URL www.cosmos.esa.int/web/csa and at NASA's CDAWeb, URL www.cdaweb.gsfc.nasa.gov.

Acknowledgments
Dartmouth UNIX specialist Terrence Kovacs contributed to software and operations at South Pole. Dartmouth engineers Mike Trimpi, Hank Harjes, and David McGaw contributed to development, construction, and maintenance of the LF/MF/HF receiving systems at South Pole; former Dartmouth graduate student Matt Broughton contributed to their deployment. The experiment owes a lot to resident South Pole technicians over the years, including Mike Legatt in 2019 and Kelly Thomas in 2020. The authors acknowledge Ivar Christopher and Robert Mutel for use of AKR beaming model software they developed, and Harald Frey and Steve Mende for summaries of South Pole optical imager data. This research was supported by National Science Foundation grant ANT-1911335 to Dartmouth College and Science and Technology Facilities Council grant ST/R000697/1 to The University of Sheffield.

References

Baumback, M. M., & Calvert, W. (1987). The minimum bandwidths of auroral kilometric radiation. *Journal of Geophysical Research*, *92*(2), 119–122. https://doi.org/10.1029/GL014i002p00119

Bilitza, D., Altadill, D., Truhlik, V., Shubin, V., Galkin, I., Reinisch, B., & Huang, X. (2017). International Reference Ionosphere 2016: From ionospheric climate to real-time weather predictions. *Space Weather*, *15*, 418–429. https://doi.org/10.1002/2016SW001593

Budden, K. G. (1988). *The propagation of radio waves* (p. 542). Cambridge: Cambridge University Press.

Burke, B. F., & Franklin, K. L. (1955). Observations of a variable radio source associated with the planet Jupiter. *Journal of Geophysical Research*, *60*(2), 213–217. https://doi.org/10.1029/JZ060i002p00213

Chian, A. C.-L., Lopes, S. R., & Alves, M. V. (1994). Generation of auroral whistler mode radiation via nonlinear coupling of Langmuir waves and Alfven waves. *Astronomy & Astrophysics*, *290*, L13–L16.

Delory, G. T., Ergun, R. E., Carlson, C. W., Muschietti, L., Chaston, C. C., Peria, W., et al. (1998). FAST observations of electron distributions within AKR source regions. *Geophysical Research Letters*, *25*(12), 2069–2072. https://doi.org/10.1029/98GL00705

Ergun, R. E., Carlson, C. W., McFadden, J. P., Delory, G. T., Strangeway, R. J., & Pritchett, P. L. (2000). Electron-cyclotron maser driven by charged-particle acceleration from magnetic field-aligned electric fields. *Astrophysical Journal*, *538*, 456–466. https://doi.org/10.1086/309094

Ergun, R. E., Carlson, C. W., McFadden, J. P., Mozer, F. S., Delory, G. T., Peria, W., et al. (1998). FAST satellite wave observations in the AKR source region. *Geophysical Research Letters*, *25*(12), 2061–2064. https://doi.org/10.1029/98GL00570

Green, J. L., Boardsen, S., Garcia, L., Fung, S. F., & Reinish, B. W. (2004). Seasonal and solar cycle dynamics of the auroral kilometric radiation source region. *Journal of Geophysical Research*, *109*, A05223. https://doi.org/10.1029/2003JA010311

Gurnett, D. A. (1974). The Earth as a radio source: Terrestrial kilometric radiation. *Journal of Geophysical Research*, *79*(28), 4227–4238. https://doi.org/10.1029/JA079i028p04227

Gurnett, D. A., & Anderson, R. R. (1981). The kilometric radio emission spectrum: Relationship to auroral acceleration processes. In Akasofu, S.-I., & Kan, J. R. (Eds.), *Physics of auroral arc formation, Geophysical Monograph Series 25* (pp. 341–350). American Geophysical Union.

Gurnett, D. A., Huff, R. L., & Kirchner, D. L. (1997). The wide-band plasma wave investigation. *Space Science Reviews*, *79*, 195–208. https://doi.org/10.1007/978-94-011-5666-0_8

Ham, Y.-B., Geonhwa, J., Lee, C., Kwon, H.-J., Kim, J.-H., Zabotin, N., & Bullett, T. (2020). Observations of the polar ionosphere by the vertical incidence pulsed ionospheric radar at Jang Bogo station, Antarctica. *Journal of Astronomy and Space Sciences*, *37*(2), 143–156. https://doi.org/10.5140/JASS.2020.37.2.143

Horne, R. B. (1995). Propagation to the ground at high latitudes of auroral radio noise below the electron gyrofrequency. *Journal of Geophysical Research*, *100*(A8), 14637–14645. https://doi.org/10.1029/95ja00633

Jones, D. (1976). The second Z-propagation window. *Nature*, *262*, 674–675. https://doi.org/10.1038/262674a0

Krasovskiy, V. L., Kushnerevskiy, Y. V., Mugulin, V. V ., Orayevskiy, V. N., & Pulinets, S. A. (1983). Ballistic wave transformation as a mechanism for the linkage of terrestrial kilometric radio waves with low frequency noise in the upper atmosphere. *Geomagnetism and Aeronomy*, *23*, 702.

Kumamoto, A., Ono, T., Iizima, M., & Oya, H. (2003). Seasonal and solar cycle variations of the vertical distribution of the occurrence probability of auroral kilometric radiation sources and of upflowing ion events. *Journal of Geophysical Research*, *108*(A1), 1032. https://doi.org/10.1029/2002JA009522

LaBelle, J. (2022). *Replication data for: South Pole station ground-based and cluster satellite measurements of leaked and escaping auroral kilometric radiation* (V1). Harvard Dataverse. https://doi.org/10.7910/DVN/TGRKJL

LaBelle, J., & Anderson, R. R. (2011). Ground-level detection of auroral kilometric radiation. *Geophysical Research Letters*, *38*, L04104. https://doi.org/10.1029/2010GL046411

LaBelle, J., McAdams, K. L., & Trimpi, M. L. (1999). High frequency and time resolution rocket observations of structured low- and medium-frequency whistler mode emissions in the auroral ionosphere. *Journal of Geophysical Research*, *104*, 28101–28107. https://doi.org/10.1029/1999JA900397

LaBelle, J., Yan, X., Broughton, M., Pasternak, S., Dombrowski, M., Anderson, R. R., et al. (2015). Further evidence for a connection between auroral kilometric radiation and ground-level signals measured in Antarctica. *Journal of Geophysical Research: Space Physics*, *120*(3), 2061–2075. https://doi.org/10.1002/2014JA020977

Melrose, D. B. (1976). An interpretation of Jupiter's radiation and the terrestrial kilometric radiation as direct amplified gyroemission. *Astrophysical Journal*, *207*, 651–662. https://doi.org/10.1086/154532

Menietti, D., Persoon, A., Pickett, J., & Gurnett, D. (2000). Statistical studies of AKR fine structure striations observed by Polar. *Journal of Geophysical Research*, *105*, 18857–18866. https://doi.org/10.1029/1999JA000389

Mutel, R. L., Christopher, I. W., Menietti, J. D., Gurnett, D. A., Pickett, J. S., Masson, A., et al. (2011). RX and Z-mode growth rates and propagation at cavity boundaries. In *Planetary radio emissions VII* (pp. 241–252). Vienna, Austria: Austrian Academy of Sciences Press.

Mutel, R. L., Christopher, I. W., & Pickett, J. S. (2008). Cluster multi-spacecraft observations of AKR angular beaming. *Geophysical Research Letters*, *35*, L07104. https://doi.org/10.1029/2008GL033377

Mutel, R. L., Gurnett, D. A., Christopher, I. W., Pickett, J., & Schlax, M. (2003). Locations of Auroral Kilometric Radiation bursts inferred from multi-spacecraft Wideband Cluster VLBI observations I: Description of technique and initial results. *Journal of Geophysical Research*, *108*, 1398. https://doi.org/10.1029/2003JA010011

Mutel, R. L., Menietti, J. D., Christopher, I. W., Gurnett, D. A., & Cook, J. M. (2006). Striated auroral kilometric radiation emission: A remote tracer of ion solitary structures. *Journal of Geophysical Research*, *111*. https://doi.org/10.1029/2006JA011660

Oya, H., & Morioka, A. (1983). Observational evidence of Z and L-O mode waves as the origin of auroral kilometric radiation from the Jikiken (EXOS-B) satellite. *Journal of Geophysical Research*, *88*(A8), 6189–6203. https://doi.org/10.1029/ja088ia08p06189

Oya, H., Morioka, A., & Obara, T. (1985). Leaked AKR and terrestrial hectometric radiations discovered by the plasma wave and sounder experiments on the EXOS-C satellite—Instrumentation and observation results of plasma wave phenomena. *Journal of Geomagnetism and Geoelectricity*, *37*, 237–262. https://doi.org/10.5636/jgg.37.237

Parrot, M., & Berthelier, J.-J. (2012). AKR-like emissions observed at low altitude by the DEMETER satellite. *Journal of Geophysical Research*, *117*(A10). https://doi.org/10.1029/2012JA017937

Pottelette, R., & Pickett, J. (2007). Phase space holes and elementary radiation events. *Nonlinear Processes in Geophysics*, *14*, 735–742. https://doi.org/10.5194/npg-14-735-2007

Pritchett, P. L., Strangeway, R. J., Carlson, C. W., Ergun, R. E., McFadden, J. P., & Delory, G. T. (1999). Free energy sources and frequency bandwidth for the auroral kilometric radiation. *Journal of Geophysical Research*, *104*(A5), 10317–10326. https://doi.org/10.1029/1998JA900179

Shutte, N., PrutenskyPulinets, I. S., Klos, Z., Rothkaehl, H., & Rothkaehl, H. (1997). The charged-particle fluxes at auroral and polar latitudes and related low-frequency auroral kilometric radiation-type and high-frequency wideband emission. *Journal of Geophysical Research*, *102*, 2105–2114. https://doi.org/10.1029/96ja01116

Wu, C. S., Dillenburg, D., Ziebell, L. F., & Freund, H. P. (1983). Excitation of whistler waves by reflected auroral electrons. *Planetary and Space Science*, *31*(5), 499–507. https://doi.org/10.1016/0032-0633(83)90041-7

Wu, C. S., & Lee, L. C. (1979). A theory of the terrestrial kilometric radiation. *Astrophysical Journal*, *230*, 621–626. https://doi.org/10.1086/157120

Wu, C. S., Yoon, P. H., & Freund, H. P. (1989). A theory of electron cyclotron waves generated along auroral field lines observed by ground facilities. *Geophysical Research Letters*, *16*(12), 1461–1464. https://doi.org/10.1029/gl016i012p01461

Yoon, P. H., Weatherwax, A. T., Rosenberg, T. J., LaBelle, J., & Shepherd, S. G. (1998). Propagation of medium frequency (1–4 MHz) auroral radio waves to the ground via the Z-mode radio window. *Journal of Geophysical Research*, *103*(A12), 29267–29275. https://doi.org/10.1029/1998JA900032

Ziebell, L. F., Wu, C. S., & Yoon, P. H. (1991). Kilometric radio waves generated along auroral field lines observed by ground facilities: A theoretical model. *Journal of Geophysical Research*, *96*(A2), 1495–1501. https://doi.org/10.1029/90ja02617